PAPER

Structure of palladium nanoparticles under oxidative conditions†

Cristina Popa,[a] Tianwei Zhu,[a] Ionut Tranca,[a] Payam Kaghazchi,[b] Timo Jacob[cd] and Emiel J. M. Hensen*[a]

Using density functional theory (DFT) and thermodynamic considerations we study the shape and stability of Pd nanoparticles in oxygen-lean and oxygen-rich atmospheres. We find that at very high oxygen coverage cubes exposing (100) faces will form, which are stabilized due to the formation of a $O/(\sqrt{5} \times \sqrt{5})R27°$ overlayer. The shape of oxygen-covered Pd and Pt nanoparticles is compared in this study.

1. Introduction

Several studies have demonstrated that the various surface orientations present on nanoparticles have a decisive impact on their activity.[1–4] Therefore, gaining insight into the shape of nanoparticles as a function of the environmental conditions is an important aspect in understanding the catalytic behavior.[47,48] Adsorbates such as oxygen can induce surface reconstructions because of substantial changes in the surface free energy. As this influences different surface orientations in an anisotropic way, it may also lead to changes in the overall particle shape. The formation of oxide layers/surface oxides on metal nanoparticles is important for heterogeneous reactions and has accordingly been investigated in detail over recent years.[5–19,22,23]

Several studies have combined experimental techniques with first-principles calculations to determine the structure of Pd-bulk oxides as well as potential surface oxides.[6,10,11,17–19,24,25,30] For instance, ordered oxygen overlayers with $p(2 \times 2)$, $c(2 \times 2)$, and $(\sqrt{5} \times \sqrt{5})R27°$ periodicities on Pd(100) have been explored by experimental[7,8,10,19,33] and theoretical[12,13,21,32] methods. The formation of the $O/(\sqrt{5} \times \sqrt{5})R27°$ overlayer structure has been argued to hinder formation of the thermodynamically favored bulk Pd-oxide. The "Persian carpet" $O/(\sqrt{6} \times \sqrt{6})Pd(111)$

structure with no bulk correspondent has also been intensively discussed. This structure was found to be the second stable surface oxide of Pd after the $(\sqrt{5} \times \sqrt{5})R27°$ structure.[6,9,10,12,13,16,20] For Pd(110), it was demonstrated that its oxidation does not proceed through a kinetically stable surface phase, but rapid bulk oxidation occurs, for which many structures have been proposed.[12,13,26,28,29,31]

There are also studies on the equilibrium shape of Pd nanoparticles in oxygen-low and oxygen-rich atmosphere.[12,26,32,33] It is usually found that these Pd nanoparticles initially form a thin oxide layer, followed by formation of bulk PdO. Due to the large amount of structures found in an oxygen-rich atmosphere for the oxygen overlayers on Pd surfaces, their consideration in Gibbs–Wulff theoretical studies have so far been limited to a small number of structures. In the present work, the Wulff construction considering the most experimentally investigated 9 Pd surfaces, with 34 possible oxygen overlayers, at both low and high oxygen coverages has been investigated. This allows to obtain a clear and consistent picture of the thermodynamic equilibrium shape of Pd nanoparticles at various oxygen pressures.

The catalytic activity of nanoparticles strongly depends on their size and the structure of the facets enclosing the particles. Under electrochemical conditions, Sun *et al.* have been able to synthesize different Pd nanoparticle shapes with high-index facets: trapezohedral shapes with {hkk} facets, concave hexoctahedral particles with {hkl} facets, fivefold-twinned nanorods, and tetrahexahedral particles dominated by {hk0} facets.[34] It was proposed that oxygen adsorption/desorption on the surfaces plays an important part in stabilizing the high-index facets during nanoparticle formation.[35] However, there is no experimental evidence to prove the relation between adsorbed oxygen species and surface stabilities.

A systematic study on the dependence of the equilibrium nanoparticle shapes on the oxygen pressure is therefore required.

[a] *Department of Chemical Engineering and Chemistry,*
 Eindhoven University of Technology, Den Dolech 2, 5612 AZ Eindhoven,
 The Netherlands. E-mail: e.j.m.hensen@tue.nl
[b] *Physical and Theoretical Chemistry, Freie Universität Berlin, Takustr. 3,*
 14195 Berlin, Germany
[c] *Institute of Electrochemistry, Ulm University, Albert-Einstein-Allee 47,*
 D-89081 Ulm, Germany
[d] *Helmholtz-Institute Ulm (HIU), Ulm University, Albert-Einstein-Allee 47,*
 D-89081 Ulm, Germany
† Electronic supplementary information (ESI) available. See DOI: 10.1039/c4cp01761g

2268 | Phys. Chem. Chem. Phys., 2015, 17, 2268–2273

This journal is © the Owner Societies 2015

In this contribution, we studied low- and high-index surfaces of Pd with a large variety of oxygen overlayers, and calculated the dependence of the surface free energy for each surface on the chemical potential of oxygen. We found that at very high oxygen coverages kinetically stable cubic nanoparticles dominated by (100) facets will form.

2. Computational details

Density functional theory (DFT) with the PBE (Perdew–Burke–Ernzerhof) functional as implemented in the Vienna ab initio Simulation Package (VASP, version 5.2.11)[36,37] was used. Spin-polarized calculations for selected cases were tested, but no significant differences were obtained with respect to the non-spin polarized calculations. Therefore, we report here the results of the non-spin polarized calculations. The projector-augmented wave method (PAW) was used to describe electron–ion interactions.[38–40]

The Pd (4p, 5s, 4d) and O (2s, 2p) electrons were treated as valence states using a plane-wave basis set with a kinetic energy cutoff of 400 eV. Van der Waals corrections (DFT-D2), as implemented by Grimme,[41] were taken into account. A calculated lattice parameter of 3.905 Å was used, which is in good agreement with the experimental value of 3.89 Å.[14] Integration in the first Brillouin zone was performed on Monkhorst–Pack k-point meshes corresponding to a $(16 \times 16 \times 1)$ mesh for the (1×1) surface cell.

The Pd surfaces were modeled by 8–10 layer slabs (the bottom layers being kept to their bulk positions) separated by a vacuum of at least 10 Å. The conjugate-gradient algorithm was used to optimize the ion positions. Atoms were relaxed until forces were smaller than 10^{-3} eV Å^{-1}. Phonon contributions of the surface and the adsorbates to the free energies have been neglected, as their effect on the relative stability of surface phases is usually small.

We are interested in the relative stability of different Pd surfaces in thermodynamic equilibrium with a gaseous environment containing O$_2$ at finite temperatures. In order to compare the thermodynamic stability of different surface phases, we calculated the energy of various Pd/O structures (see Table 1) and used the corresponding energetics together with the *ab initio* atomistic thermodynamics approach, which for example is described in ref. 42 and 43 in detail.

The surface energy is calculated as

$$\gamma(\mu_{Me}, \mu_O) = \frac{1}{A}(E_{total} - N_{Me} \cdot \mu_{Me} - N_O \cdot \mu_O) - \gamma_{bare}(\mu_{Me}) \quad (1)$$

where A is the surface area, E_{total} the total slab energy (including the adlayers), N_{Me} and N_O are the number of metal and oxygen atoms, respectively. The surface energy of the relaxed bare surface, γ_{bare}, is subtracted due to the slab approach used in the calculations (one side bare, second side oxygen covered). The chemical potential of the metal atoms, μ_{Me}, is fixed to the formation energy of the bulk phase, while the oxygen

Table 1 Details of the surface O/Pd structures employed in this study

Surface	Unit cell of oxygen overlay	N_{layers}/$N_{fixed\text{-}layers}$	Surface orientation
Pd(100)	$(\sqrt{5} \times \sqrt{5})R27°$	9/4	(100)
	$p(2 \times 2)$	8/4	
	$c(2 \times 2)$	8/4	
Pd(111)	$(\sqrt{6} \times \sqrt{6})$	7/2	(111)
	O$_{fcc,hpc}$/$p(2 \times 2)$	6/3	
Pd(110)	(10×2)	10/6	(110)
	(1×3)	10/6	
	(2×1)-2O	10/6	
	(2×2)-p2mg^a	10/6	
	(2×3)-1D^b	10/6	
	(2×3)-deep-O^c	10/6	
	(3×2)	10/6	
	$(7 \times \sqrt{3})$	10/6	
	$(9 \times \sqrt{3})$	10/6	
	$c(2 \times 4)$	10/6	
	$p(2 \times 2)$	10/6	
Pd(211)	O$_{fcc}$/(1×2)	8/4	3(111)-(100)
	2O/(1×2)	8/4	
Pd(311)	(2×4)-MR-0.5 ML^d	10/5	2(100)-(111)
	(2×4)-MR-1 ML	10/5	
Pd(331)	1O	8/4	3(111)-(111)
	2O	8/4	
Pd(210)	1O	5/3	2(100)-(110)
	2O	5/3	
	7O	5/3	
	8O	5/3	
Pd(520)	1O	5/3	3(100)-(110) + 2(100)-(110)
	2O	5/3	
	4O	5/3	
	6O	5/3	
	10O	5/3	
Pd(730)	1O	5/3	(520) + (210)
	3O	5/3	
	9O	5/3	

^{a} Zig-zag structure. ^{b} Double missing-row structure. ^{c} Row missing in the next palladium layer. ^{d} Missing row.

gas reservoir is described by its chemical potential referenced as follows:

$$\mu_O = \frac{1}{2}[E_{O_2}^{tot}] + \Delta\mu_O \quad (2)$$

The binding energy per O atom in O$_2$ is calculated to be 3.06 eV per atom and the bond distance 1.235 Å. These values are typical of well-converged DFT-GGA calculations; similar values have been obtained by, *e.g.*, Perdew *et al.*[53] The experimental results are 2.59 eV per atom and 1.207 Å, respectively.[52]

The binding energy of O$_2$ is overestimated by more than 0.5 eV using some of the most popular GGA functionals. This error can lead to deviations in the absolute values of the surface energies. However, the trends in surface stabilities will be essentially correct. The size of the systems described here prohibits the use of accurate wave-function based *ab initio* methods.

This journal is © the Owner Societies 2015

Phys. Chem. Chem. Phys., 2015, **17**, 2268–2273 | **2269**

The oxygen chemical potential is related to temperature and pressure by assuming that the surface is in thermodynamic equilibrium with the gas phase. As the surrounding O_2 atmosphere forms an ideal gas reservoir, the pressure and temperature dependence of $\Delta\mu_O(T,p)$ can be determined by

$$\Delta\mu_O(T, p_{O_2}) = \frac{1}{2}\left[H(T, p^0) - H(0\,K, p^0) - T \cdot S(T, p^0) \right.$$
$$\left. + RT \ln\left(p_{O_2}/p^0\right) \right],$$

where p^0 is the pressure of a reference state (1 atm). For the enthalpy H and the entropy S we use tabulated values from the JANAF thermodynamics tables.[45]

3. Results and discussion

3.1 Structures and relative stabilities

To determine the most favorable O/Pd surfaces under particular conditions, we consider adsorption of different oxygen overlayers on the Pd surfaces (listed in Table 1). Among all structures, higher coverage adlayers ($\theta_O = 0.5$–0.9 ML) with strong oxygen adsorption energies are found to be most favorable. These involve substantial roughening of the first atomic metal layers. On the Pd(100) surface, the most stable structure is $4O/(\sqrt{5} \times \sqrt{5})R27^\circ$ (see Fig. 1a). In the unit cell of this structure two O atoms prefer being located below and two atoms above the first Pd layer, so as to form an O–Pd–O trilayer. This two-dimensional oxide surface has the same lattice as the PdO(101) surface (Fig. 1b), as the first one grows epitaxial towards the latter one.[13] Despite the structural similarity, the electronic properties of these surfaces are different. On the Pd(111) surface, the most stable structure among all the coverages that we investigated for Pd(111) involves a $(\sqrt{6} \times \sqrt{6})$ arrangement of O atoms with the Pd_4O_5 stoichiometry (Fig. 1c). Also in this unit cell, there is a strong surface reconstruction, and four O atoms coordinate in plane to the surface Pd atoms. On the Pd(110) surface, adlayers with higher oxygen surface coverages are the more stable ones (e.g., $p(10 \times 2)$, $(7 \times \sqrt{3})$, $c(2 \times 4)$) (Fig. 1d), but they are only loosely related to the bulk PdO structure. In order to compare

these structures with the stable ones obtained upon oxygen adsorption on Pt(210), Pt(520) and Pt(730),[35] we computed similar structures for Pd as well (Fig. 2).
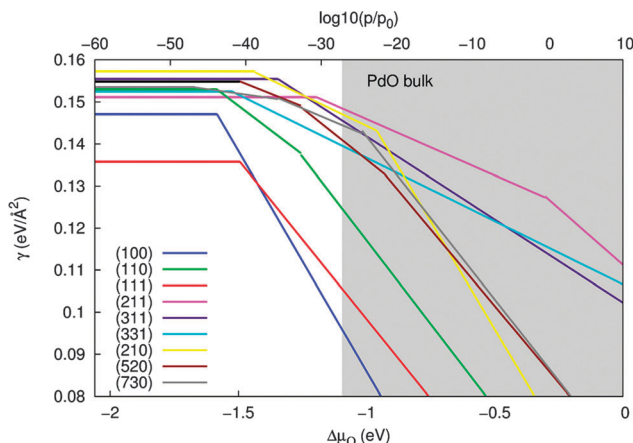
Fig. 2 Stability plot for the oxidation of Pd surfaces showing the surface stability γ as function of the oxygen chemical potential ($\Delta\mu_O$) at room temperature ($T = 300$ K). The region at which the bulk oxide (PdO) is stable is indicated in grey. The type of the oxygen overlayer found at different $\Delta\mu_O$ intervals is given in Table 2.

Table 2 Oxygen chemical potential ranges at which the O/Pd surfaces are stabilized ($T = 300$ K) corresponding to the stability plot (Fig. 3)

Surface	$\Delta\mu_O$ range (eV)	Structure
Pd(100)	$-2.06\ldots-1.58$	Clean surface
	$-1.58\ldots0$	$(\sqrt{5} \times \sqrt{5})R27^\circ$
Pd(111)	$-2.06\ldots-1.49$	Clean surface
	$-1.49\ldots0$	$(\sqrt{6} \times \sqrt{6})$
Pd(110)	$-2.06\ldots-1.58$	Clean surface
	$-1.58\ldots-1.26$	$c(2 \times 4)$
	$-1.26\ldots-0.39$	$(7 \times \sqrt{3})$
	$-0.39\ldots0$	(10×2)
Pd(211)	$-2.06\ldots-1.19$	Clean surface
	$-1.19\ldots-0.30$	1O
	$-0.30\ldots0$	2O
Pd(311)	$-2.06\ldots-1.34$	Clean surface
	$-1.34\ldots0$	(2×4)-MR-0.5 ML
Pd(331)	$-2.06\ldots-1.52$	Clean surface
	$-1.52\ldots0$	1O
Pd(210)	$-2.06\ldots-1.43$	Clean surface
	$-1.43\ldots-0.96$	2O
	$-0.96\ldots0$	7O
Pd(520)	$-2.06\ldots-1.49$	Clean surface
	$-1.49\ldots-1.26$	2O
	$-1.26\ldots-0.92$	4O
	$-0.92\ldots0$	6°
Pd(730)	$-2.06\ldots-1.67$	Clean surface
	$-1.67\ldots-1.34$	1O
	$-1.34\ldots-1.02$	3O
	$-1.02\ldots0$	9°

O/($\sqrt{5}\times\sqrt{5}$)R27° Pd(100)
$\Theta = 0.8$ ML

PdO(101)(2x1)

($\sqrt{6}$x$\sqrt{6}$)Pd(111)
$\Theta = 0.69$ ML

$p(10$x$2)$ Pd(110)
$\Theta = 0.9$ ML

$(7$x$\sqrt{3})$Pd(110)
$\Theta = 0.86$ ML
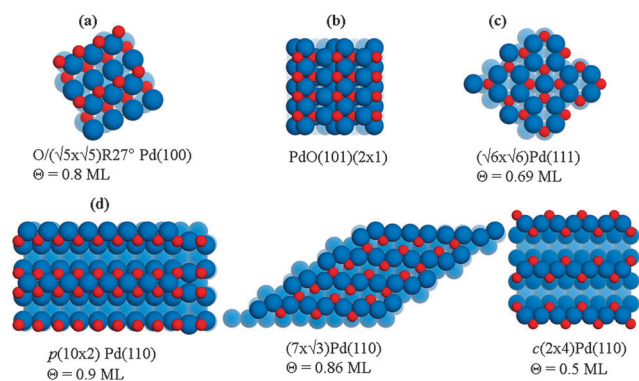
$c(2$x$4)$Pd(110)
$\Theta = 0.5$ ML

Fig. 1 Top views of the most stable structures with different oxygen coverages of (a) Pd(100), (b) PdO, (c) Pd(111) and (d) Pd(110) reconstructed surfaces. The other computed structures are depicted in the ESI.†

3.2 Thermodynamics

In order to determine the stability of the various surface structures under the influence of oxygen, we show in Fig. 2 the surface free energies as function of the oxygen chemical potential, $\Delta\mu_O$. Each line corresponds to a particular Pd/O surface adlayer structure. We mainly focus on O adsorption on the pure Pd surface at chemical potentials below -1.09 eV before PdO bulk oxide is stabilized (indicated by the grey area). As O adatoms typically have stronger interaction with metal surfaces than water or hydroxyl groups,[40] we focus in this work on the influence of O atoms, as we expect that adsorbate-induced restructuring requires strongly interacting adsorbates.[44]

The stability plot shows that, for each Pd surface below a critical $\Delta\mu_O$ where no O is adsorbed on the surface, the surface free energy remains constant (horizontal lines). Above this critical value, O adlayers start to form on the surfaces, resulting in decreased surface free energy (γ) when increasing the oxygen chemical potential, where the O coverage increases gradually with $\Delta\mu_O$. The higher the coverage is, the steeper the slope. As expected, among the clean surfaces the densest one has the lowest surface free energy, i.e., Pd(111) followed by Pd(100). The other surfaces have surface free energies between 151 and 157 meV $Å^{-1}$. This is consistent with the shapes reported for pure Pd nanoparticles, e.g., tetrahedra, octahedra, decahedra, and icosahedra, which are enclosed by (111) facets.[44,46] We should note that experimentally also Pd nanoparticles with a spherical shape composed of (110) and other high-index (210), (211), (311) and (730) facets have been observed.[27,34]

Above $\Delta\mu_O = -1.67$ eV, O adsorption starts on the various Pd surfaces (non-horizontal lines). Adsorption occurs at the lowest chemical potential for Pd(730) because of the higher coordinative unsaturation of the Pd surface metal atoms compared to those in Pd(110) and Pd(100) surfaces. The difference is, however, relatively small. Above $\Delta\mu_O = -1.58$ eV, O starts to adsorb on the other Pd surfaces. The clean Pd(111) surface is the most stable structure up to $\Delta\mu_O = -1.49$ eV, where O starts to adsorb on the (111) surface forming a $(\sqrt{6} \times \sqrt{6})$ surface structure. At about this chemical potential, the $(\sqrt{5} \times \sqrt{5})R27°$-O/Pd(100) structure becomes the most stable surface structure among all the studied oxygen adlayers, and remains to be the most stable one compared to all the other O-covered surfaces for higher chemical potential.

At high oxygen coverages, the open surfaces still have relatively high surface free energies compared to the low-index surfaces. Pd(210), Pd(520) and Pd(730), which all have similar surface topologies, also exhibit similar stabilities at low oxygen chemical potentials, consistent with results reported for similar Pt surfaces.[11] At higher chemical potentials, the anisotropy between these orientations increases (Fig. 2).

3.3 Pd nanoparticles formation

Nanoparticles' modelling, their morphology and evolution are well debated problems, and many theoretical and computational studies were devoted to explore structure–property relationships at the nanoscale.[54] The size of the nanoparticles determines

the selectivity of the nanoparticle shapes.[55] The equilibrium shape is determined by minimization of the overall Gibbs free energy, which is mainly the sum of surface, edge, corner, and strain contributions. For smaller nanoparticles, the strains given by the apexes and edges are significant, and having very small terraces may result in shapes that include higher index surfaces with high surface energies. Strain contributions slowly converge to the bulk values with increasing particle size and, for larger particles ($d > 3$–5 nm), they are diminished. In this size range, the shape can be determined by application of the Gibbs–Wulff theorem.[49] The formation is dominated by the surface contributions only and the equilibrium shape can be obtained by

$$\min \sum_i \gamma_i A_i \qquad (4)$$

where γ_i and A_i are the surface free energy and the area of the facet i of the particle, respectively. The Wulff construction predicts a particle with a constant ratio between the surface energy γ_i and the distance d_i from the surface i to the center of the nanoparticle, that is

$$\gamma_i/d_i = \text{const.} \qquad (5)$$

Our calculations point out that for larger nanoparticles ($d > 3$–5 nm), the Pd nanoparticles are mainly truncated octahedrons, while smaller nanoparticles have higher index facets as well. Moreover, the equilibrium shape changes under oxidizing conditions, due to the oxygen chemical potential influence over the surface energy. We use the low-index Pd(111), (100), and (110), as well as the high-index (210), (211), (311), (331), (520), and (730) surfaces, with and without oxygen to construct the equilibrium shapes of Pd nanoparticles. Using the computed values of γ_i, we modeled Pd nanoparticles satisfying eqn (4) as a function of selected values of $\Delta\mu_O$ (Fig. 3).

The results presented here are representative for particles that have the truncated octahedron shape in the absence of the oxygen. The calculations performed for smaller nanoparticles indicate that the higher index surfaces are changing faster with the increase of the oxygen chemical potential, i.e., leading to complete oxidized nanoparticles.

From Fig. 2, one can already notice that the close-packed clean surfaces have the highest stabilities in the absence
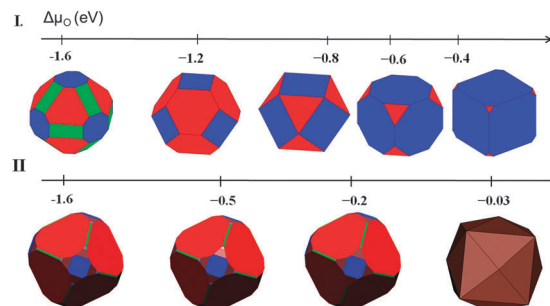

Fig. 3 Equilibrium shape of (top) Pd and (bottom) Pt nanoparticles as a function of the chemical potential of O at room temperature (blue: (100), red: (111), green: (110), brown: (520) surfaces).

of oxygen. Fig. 3 shows that at low potentials with no O adsorbed the nanoparticle is mainly enclosed by close-packed (111) facets with the lowest surface free energy among all of the surfaces as well as small contributions from (100) and (110) facets. These latter facets are the second and third most stable surfaces according to the stability plot (Fig. 2). After increasing the oxygen chemical potential above −1.36 eV, the (111) and (100) facets with $(\sqrt{6} \times \sqrt{6})$-O and $(\sqrt{5} \times \sqrt{5})R27°$-O overlayers have the highest contribution to the surface of Pd nanoparticles (Fig. 3). This result is in agreement with UHV experiments, showing that after O adsorption Pd nanoparticles reach an equilibrium shape enclosed by (100) and (111) facets.[50] As already mentioned, when the oxygen chemical potential increases to −1.36 eV, the $(\sqrt{5} \times \sqrt{5})R27°$-O/Pd(100) structure becomes the most stable one among all studied O-covered adlayers. In addition, we found that the higher the potential is, the larger the difference of the surface free energies between $(\sqrt{5} \times \sqrt{5})R27°$-O/Pd(100) and other O-adsorbed surfaces is. Fig. 3 shows that, at $\Delta\mu_O$ = −0.40 eV, the shape of the nanoparticle is almost cubic with dominant (100) facets and only a small fraction of (111) facets. This result is in agreement with experiments that show that Pd cubic nanoparticles are mainly enclosed by Pd(100) facets.[34] Although from our stability plot the PdO bulk oxide becomes thermodynamically stable for $\Delta\mu_O$ > −1.09 eV, there is no experimental evidence for the formation of PdO nanoparticles at these chemical potentials. Therefore, cubic-like Pd nanoparticles represent meta-stable phases, likely stabilized as a result of kinetic limitations in the formation of the PdO bulk oxide.

Fig. 3 shows that none of the recently experimentally observed Pd nanoparticles under electrochemical conditions such as trapezohedral, concave hexoctahedral, nanorods, or tetrahexahedral are thermodynamically stable. However, trapezohedral, concave hexoctahedral, and tetrahexahedral particles with {hkk}, {hkl} and {hk0} facets, respectively, have been observed at relatively high oxygen chemical potential values.[51] The $(\sqrt{5} \times \sqrt{5})R27°$-O/Pd(100) structure with a strongly reconstructed surface grows epitaxially towards the PdO(101) surface and the thermodynamic barrier of this process could explain the kinetic stability of metallic Pd nanoparticles containing the above-mentioned surface facets. This is essentially the most stable oxidized surface Pd structure. Therefore, a kinetically stabilized nanoparticle at relatively low oxygen chemical potential will expose $(\sqrt{5} \times \sqrt{5})R27°$-O/Pd(100) facets.

In a previous study, we discussed the shape of oxygen-covered Pt nanoparticles.[35] Clean Pd and Pt nanoparticles exhibit similar shapes (see Fig. 3). At higher potential, Pt forms tetrahexahedral nanoparticles, while Pd prefers cubic nanoparticle shapes. At higher potentials, where adlayers with high O coverage are formed, well-shaped nanoparticles bound with only one or two types of exposed facets are most stable. Bulk PdO formation takes place at a lower oxygen chemical potential (−1.09 eV) than bulk PtO_2 formation (−0.9 eV),[35] consistent with the higher binding energy of O to Pd. Moreover, in the case of Pd, all low index surfaces oxidize with high O coverages at lower $\Delta\mu_O$ values,

and the stepped surfaces are less stable, whereas for Pt the stepped surfaces, such as (210), (520), (730) are stable and consequently Pt nanoparticles contain such facets. This explains why for larger $\Delta\mu_O$ values (i.e., high O coverages) Pt nanoparticles have high index facets (520), while Pd nanoparticles mainly expose $(\sqrt{5} \times \sqrt{5})R27°$-O/Pd(100) (0.8 ML) and small areas of $(\sqrt{6} \times \sqrt{6})$-O/Pd(111) (0.69 ML) facets.

4. Conclusions

We have investigated clean and O covered low- and high-index surfaces of Pd using DFT calculations. The surface stability data were used in a thermodynamic analysis to predict nanoparticle shapes as function of O coverages. At low chemical potential, where no O is adsorbed, Pd(111) is the most stable surface. Under these conditions the preferred shape of the Pd nanoparticle is a polyhedron consisting mainly of (111) and (100) facets. Upon increasing the potential an O-covered Pd(100) (θ = 0.8 ML) becomes the most stable surface. Surface roughening is much more drastic for the Pd(100) surface than the other surfaces. On Pd(100), O adatoms form a square overlayer to reduce the O–O repulsions. This surface has the same structure as the first surface layer of PdO(101). Under these conditions, cubic-shaped particles enclosed with (100) facets may form as a metastable structure. The present results are not fully applicable to Pd nanoparticles smaller than 5 nm. A comparison is made between the faceting of Pd and Pt nanoparticles under oxidative conditions.

Acknowledgements

References

1 R. A. van Santen, M. Neurock and S. G. Shetty, *Chem. Rev.*, 2010, **110**, 2005.
2 N. Lopez, T. V. W. Janssens, B. S. Clausen, Y. Xu, M. Mavrikakis, T. Bligaard and K. Nørskov, *J. Catal.*, 2004, **223**, 232.
3 A. Ueda and M. Haruta, *Gold Bull.*, 1999, **32**, 3.
4 N. Tian, Z. Y. Zhou and S. G. Sun, *J. Phys. Chem. C*, 2008, **112**, 19801.
5 M. J. Peuckert, *Phys. Chem.*, 1985, **89**, 2481.
6 E. Lundgren, G. Kresse, C. Klein, M. Borg, J. N. Andersen, M. De Santis, Y. Gauthier, C. Konvicka, M. Schmid and P. Varga, *Phys. Rev. Lett.*, 2002, **88**, 246103.
7 G. Zheng and E. I. Altman, *Surf. Sci.*, 2002, **504**, 253.

8 A. Stierle, N. Kasper, H. Dosch, E. Lundgren, J. Gustafson, A. Mikkelsen and J. N. Andersen, *J. Chem. Phys.*, 2005, **122**, 044706.

9 M. Todorova, K. Reuter and M. Scheffler, *Phys. Rev. B: Condens. Matter Mater. Phys.*, 2005, **71**, 195403.

10 E. Lundgren, A. Mikkelsen, J. Andersen, G. Kresse, M. Schmid and P. Varga, *J. Phys.: Condens. Matter*, 2006, **18**, R481.

11 P. Kostelnìk, N. Seriani, G. Kresse, A. Mikkelsen, E. Lundgren, V. Blum, T. Šikola, P. Varga and M. Schmid, *Surf. Sci.*, 2007, **601**, 1574.

12 F. Mittendorfer, N. Seriani, O. Dubay and G. Kresse, *Phys. Rev. B: Condens. Matter Mater. Phys.*, 2007, **76**, 233413.

13 N. Seriani and F. Mittendorfer, *J. Phys.: Condens. Matter*, 2008, **20**, 184023.

14 H. Graoui, S. Giorgio and C. R. Henry, *Surf. Sci.*, 1998, **417**, 350.

15 H. Graoui, S. Giorgio and C. R. Henry, *Philos. Mag. B*, 2001, **81**, 1649.

16 G. Kresse, W. Bergermayer, R. Podloucky, E. Lundgren, R. Koller, M. Schmid and P. Varga, *Appl. Phys. A*, 2003, **76**, 701.

17 R. Westerström, J. Gustafson, A. Resta, A. Mikkelsen, J. N. Andersen, E. Lundgren, N. Seriani, F. Mittendorfer, M. Schmid, J. Klikovits, P. Varga, M. D. Ackermann, J. W. M. Frenken, N. Kasper and A. Stierle, *Phys. Rev. B: Condens. Matter Mater. Phys.*, 2007, **76**, 155410.

18 F. Mittendorfer, *J. Phys.: Condens. Matter*, 2010, **22**, 393001.

19 E. Lundgren, J. Gustafson, A. Mikkelsen, J. N. Andersen, A. Stierle, H. Dosch, M. Todorova, J. Rogal, K. Reuter and M. Scheffler, *Phys. Rev. Lett.*, 2004, **92**, 046101.

20 J. Klikovits, E. Napetschnig, M. Schmid, N. Seriani, O. Dubay, G. Kresse and P. Varga, *Phys. Rev. B: Condens. Matter Mater. Phys.*, 2007, **76**, 045405.

21 J. Rogal, K. Reuter and M. Scheffler, *Phys. Rev. Lett.*, 2007, **98**, 046101.

22 R. Westerström, C. J. Weststrate, A. Resta, A. Mikkelsen, J. Schnadt, J. N. Andersen, E. Lundgren, M. Schmid, N. Seriani, J. Harl, F. Mittendorfer and G. Kresse, *J. Phys.: Condens. Matter*, 2008, **20**, 184018.

23 J. Zhou, A. P. Baddorf, D. R. Mullins and S. H. Overbury, *J. Phys. Chem. C*, 2008, **112**, 9336.

24 A. Dianat, N. Seriani, M. Bobeth, W. Pompe and L. C. Ciacchi, *J. Phys. Chem. C*, 2008, **112**, 13623.

25 A. Dianat, J. Zimmermann, N. Seriani, M. Bobeth, W. Pompe and L. C. Ciacchi, *Surf. Sci.*, 2008, **602**, 876.

26 M. Kralj, T. Pertram, N. Seriani, F. Mittendorfer, A. Krupski, C. Becker and K. Wandelt, *Surf. Sci.*, 2008, **602**, 3706.

27 D. Farías, M. Patting and K. H. Rieder, *Surf. Sci.*, 1997, **385**, 115.

28 H. Niehus and C. Achete, *Surf. Sci.*, 1996, **369**, 9.

29 H. Tanaka, J. Yoshinobu and M. Kawai, *Surf. Sci.*, 1995, **327**, L505.

30 H. H. Kan and J. F. Weaver, *Surf. Sci.*, 2008, **602**, L53.

31 R. Westerström, C. J. Weststrate, J. Gustafson, A. Mikkelsen, J. Schnadt, J. N. Andersen, E. Lundgren, N. Seriani, F. Mittendorfer, G. Kresse and A. Stierle, *Phys. Rev. B: Condens. Matter Mater. Phys.*, 2009, **80**, 125431.

32 N. Seriani, J. Harl, F. Mittendorfer and G. Kresse, *J. Chem. Phys.*, 2009, **131**, 054701.

33 R. Westerström, M. E. Messing, S. Blomberg, A. Hellman, H. Grönbeck, J. Gustafson, N. M. Martin, O. Balmes, R. van Rijn, J. N. Andersen, K. Deppert, H. Bluhm, Z. Liu, M. E. Grass, M. Hävecker and E. Lundgren, *Phys. Rev. B: Condens. Matter Mater. Phys.*, 2011, **83**, 115440.

34 N. Tian, Z. Y. Zhou and S. G. Sun, *Chem. Commun.*, 2009, 1502.

35 T. Zhu, E. J. M. Hensen, R. A. van Santen, N. Tian, S. G. Sun, T. Jacob and P. Kaghazchi, *Phys. Chem. Chem. Phys.*, 2013, **15**, 2268.

36 G. Kresse and J. Furthmuller, *Phys. Rev. B: Condens. Matter Mater. Phys.*, 1996, **54**, 11169.

37 G. Kresse and J. Furthmuller, *Comput. Mater. Sci.*, 1996, **6**, 15.

38 O. Bengone, M. Alouani, P. Blochl and J. Hugel, *Phys. Rev. B: Condens. Matter Mater. Phys.*, 2000, **62**, 16392.

39 P. E. Blochl, *Phys. Rev. B: Condens. Matter Mater. Phys.*, 1994, **50**, 17953.

40 G. Kresse and D. Joubert, *Phys. Rev. B: Condens. Matter Mater. Phys.*, 1999, **59**, 1758.

41 S. J. Grimme, *Comp. Chem.*, 2006, **27**, 1787.

42 K. Reuter and M. Scheffler, *Phys. Rev. B: Condens. Matter Mater. Phys.*, 2001, **65**, 035406.

43 P. Kaghazchi and T. Jacob, *Phys. Rev. B: Condens. Matter Mater. Phys.*, 2007, **76**, 245425.

44 K. Reuter and M. Scheffler, *Phys. Rev. B: Condens. Matter Mater. Phys.*, 2001, **65**, 035406.

45 *JANAF* Thermochemical Tables, ed. D. R. Stull and H. Prophet, U.S. National Bureau of Standards, Washington D.C., 1971.

46 T. E. Madey, W. Chen, H. Wang, P. Kaghazchi and T. Jacob, *Chem. Soc. Rev.*, 2008, **37**, 2310.

47 T. S. Ahmadi, Z. L. Wang, T. G. Green, A. Henglein and M. A. El-Sayed, *Science*, 1996, **272**, 1924.

48 F. Kim, S. Connor, H. Song, T. Kuykendall and P. D. Yang, *Angew. Chem., Int. Ed.*, 2004, **43**, 3673.

49 G. Wulff, *Z. Kristallogr.*, 1901, **34**, 449.

50 Y. J. Xiong, J. M. Mclellan, Y. D. Yin and Y. N. Xia, *Angew. Chem., Int. Ed.*, 2007, **46**, 790.

51 H. Graoui, S. Giorgio and C. R. Henry, *Surf. Sci.*, 1998, **417**, 350.

52 G. Herzberg, *Molecular Spectra and Molecular Structure. I. Spectra of Diatomic Molecules*, Krieger, Malabar, FL, 1989.

53 J. P. Perdew, K. Burke and M. Ernzerhof, *Phys. Rev. Lett.*, 1996, **77**, 3865.

54 A. S. Barnard, *Rep. Prog. Phys.*, 2010, **73**, 086502.

55 A. S. Barnard, *Catal. Sci. Technol.*, 2012, **2**, 1485.

This journal is © the Owner Societies 2015

Phys. Chem. Chem. Phys., 2015, **17**, 2268–2273 | 2273